Theoretical and numerical study of axisymmetric lattice Boltzmann models

Haibo Huang* and Xi-Yun Lu

Department of Mechanical Engineering, University of Science and Technology of China, Hefei 230026, China

(Received 6 February 2009; revised manuscript received 15 April 2009; published 8 July 2009)

The forcing term in the lattice Boltzmann equation (LBE) is usually used to mimic Navier-Stokes equations with a body force. To derive axisymmetric model, forcing terms are incorporated into the two-dimensional (2D) LBE to mimic the additional axisymmetric contributions in 2D Navier-Stokes equations in cylindrical coordinates. Many axisymmetric lattice Boltzmann D2Q9 models were obtained through the Chapman-Enskog expansion to recover the 2D Navier-Stokes equations in cylindrical coordinates [I. Halliday *et al.*, Phys. Rev. E **64**, 011208 (2001); K. N. Premnath and J. Abraham, Phys. Rev. E **71**, 056706 (2005); T. S. Lee, H. Huang, and C. Shu, Int. J. Mod. Phys. C **17**, 645 (2006); T. Reis and T. N. Phillips, Phys. Rev. E **75**, 056703 (2007); J. G. Zhou, Phys. Rev. E **78**, 036701 (2008)]. The theoretical differences between them are discussed in detail. Numerical studies were also carried out by simulating two different flows to make a comparison on these models' accuracy and τ sensitivity. It is found all these models are able to obtain accurate results and have the second-order spatial accuracy. However, the model C [J. G. Zhou, Phys. Rev. E **78**, 036701 (2008)] is the most stable one in terms of τ sensitivity. It is also found that if density of fluid is defined in its usual way and not directly relevant to source terms, the lattice Boltzmann model seems more stable.

DOI: 10.1103/PhysRevE.80.016701 PACS number(s): 47.11.−j

I. INTRODUCTION

The lattice Boltzmann method (LBM) has been proposed as an alternative numerical scheme for solving the incompressible Navier-Stokes (NS) equations [1,2]. The forcing term or source term is usually added to the lattice Boltzmann equation (LBE) to mimic Navier-Stokes equations with a body force [3–5].

To avoid three-dimensional (3D) simulation and simulate the axisymmetric flow more efficiently, the forcing-term strategy is also applied to derive the two-dimensional (2D) axisymmetric LBM [6–12]. To mimic the additional axisymmetric contributions in 2D Navier-Stokes equations in cylindrical coordinates, several spatial and velocity-dependent source terms were proposed to insert into the common LBE [6].

However, in the derivation of Halliday *et al.* [6], some important terms are not considered in their derivation. Hence, the model is not able to recover the NS equation at the macroscopic level correctly and it can only give poor simulation results for fluid flows in constricted or expended tubes [7]. If the swirl velocity is not considered, the model of Peng *et al.* [8] is identical as that of Halliday *et al.* [6].

Later, Lee *et al.* [7] and Reis and Phillips [9,10] also derived modified axisymmetric D2Q9 models following the same procedure of Halliday *et al.* [6]. The revised axisymmetric D2Q9 model proposed by Lee *et al.* [7] is able to recover the NS equation correctly. These models [6–10] are basically identical because their derivation procedures are the same. In Appendix A, the models of Reis and Phillips [9] and Lee *et al.* [7] are proven basically identical, although they are obtained independently. Minor differences between them are also illustrated. This kind of derivation procedure hereafter is referred as method A. Model of Lee *et al.* [7] hereafter is referred as model A.

In method A, the derivation begins from the common LBE and the density of fluid and velocity are defined as their usual way. While through applying a different derivation strategy (referred as method B), Premnath and Abraham [11] obtained another model. In the derivation, the trapezium rule was used to integrate the Boltzmann equation and forcing term was written in a fixed form $S_i=\frac{F_\alpha(e_{i\alpha}-u_\alpha)}{\rho RT}f_i^{eq}$ [13], which includes the equilibrium distribution function (EDF). This model here is referred as model B1. On the other hand, the forcing term S_i can also be written in a power series in the particle velocity [14] and the density of fluid can be defined as usual [4]. Following the same derivation procedure (i.e., method B), we can also obtain a model referred as B2.

In the above models, the second source term involves more complicated terms which are of $O(u^3)$ [12]; that is, inconsistent with the LBM. To solve the problem, Zhou [12] introduced a centered scheme [15] for both the first and second source terms. The strategy (hereafter it is referred as method C) makes the derivation procedure much simpler and the added source terms looks more concise and simple.

In this paper, the theoretical difference between these three-type models [6–9,11,12] would be analyzed in detail. Numerical studies on two different flows with three curved-wall boundary treatments [16–18] were also carried out to make a comparison on accuracy and seek which model is more stable in terms of τ sensitivity.

II. THEORETICAL STUDY

A. Three-type forcing strategies and models

Here, we consider the axisymmetric flows of an incompressible liquid with an axis in the x direction. The continuity (1) and Navier-Stokes momentum (2) in the pseudo-Cartesian coordinates (x,r) are used to describe the flow in axial and radial directions [19],

$$\partial_\beta u_\beta = -\frac{u_r}{r}, \tag{1}$$

*huanghb@ustc.edu.cn

$$\partial_t u_\alpha + \partial_\beta(u_\beta u_\alpha) + \frac{1}{\rho}\partial_\alpha p - \nu\partial_\beta(\partial_\beta u_\alpha) = -\frac{u_\alpha u_r}{r} + \frac{\nu}{r}\left(\partial_r u_\alpha - \frac{u_r}{r}\delta_{\alpha r}\right), \quad (2)$$

where $u_\beta(\beta=x,r)$ is the two components of velocity. u_α is the velocity u_x or u_r. It should notice that the LB models considered in this paper are all limited to nonswirling flows. In the following descriptions, the source term $S_i=S_i^{(1)}+\delta_t S_i^{(2)}$ would be incorporated into the 2D LBE to mimic the additional axisymmetric contributions in 2D Navier-Stokes equations in cylindrical coordinates. $S_i^{(1)}$ and $S_i^{(2)}$ are the first and second source terms, respectively.

For method A, the LBE is in its usual way and a forcing term is added directly on the right-hand side of LBE as

$$f_i(\mathbf{x}+\mathbf{e}_i\delta_t, t+\delta_t) - f_i(\mathbf{x},t) = -\frac{f_i - f_i^{eq}}{\tau} + \delta_t S_i(\mathbf{x},t). \quad (3)$$

In Eq. (3), $\mathbf{e}_i$'s are the discrete velocities. For the D2Q9 model, they are given by

$$[\mathbf{e}_0,\mathbf{e}_1,\mathbf{e}_2,\mathbf{e}_3,\mathbf{e}_4,\mathbf{e}_5,\mathbf{e}_6,\mathbf{e}_7,\mathbf{e}_8] = c\begin{bmatrix} 0 & 1 & 0 & -1 & 0 & 1 & -1 & -1 & 1 \\ 0 & 0 & 1 & 0 & -1 & 1 & 1 & -1 & -1 \end{bmatrix}.$$

The equilibrium distribution function is defined as

$$f_i^{eq}(\mathbf{x},t) = \omega_i\rho\left[1 + \frac{e_{i\alpha}u_\alpha}{c_s^2} + \frac{u_\alpha u_\beta}{2c_s^2}\left(\frac{e_{i\alpha}e_{i\beta}}{c_s^2} - \delta_{\alpha\beta}\right)\right]. \quad (4)$$

For the D2Q9 model, $\omega_i=4/9$ $(i=0)$, $\omega_i=1/9$, $(i=1,2,3,4)$, $\omega_i=1/36$, $(i=5,6,7,8)$, $c_s=\frac{c}{\sqrt{3}}$, where $c=\frac{\delta_x}{\delta_t}$ is the ratio of lattice spacing δ_x and time step δ_t.

The macrovariables are defined as

$$\rho u_\alpha = \sum_i e_{i\alpha}f_i = \sum_i e_{i\alpha}f_i^{eq}, \quad \rho = \sum_i f_i = \sum_i f_i^{eq}. \quad (5)$$

Through the Chapman-Enskog expansion, we know $f_i=f_i^{(0)}+\delta_t f_i^{(1)}+\delta_t^2 f_i^{(2)}$ and the distribution function $f_i^{(0)}, f_i^{(1)}, f_i^{(2)}$ is constrained by the following relationships:

$$\sum_{i=0}^{8} f_i^{(0)} = \frac{p}{c_s^2} = \rho, \quad \sum_{i=0}^{8} e_{i\alpha}f_i^{(0)} = \rho u_\alpha, \quad (6)$$

$$\sum_{i=0}^{8} f_i^{(k)} = 0, \quad \sum_{i=0}^{8} e_{i\alpha}f_i^{(k)} = 0 \quad (\text{for } k>0). \quad (7)$$

Applying the Chapman-Enskog expansion, to recover NS equations, the constraints for source terms can be obtained (refer to the Appendix A). The expression of $S_i^{(1)}, S_i^{(2)}$ are derived as [7]

$$S_i^{(1)} = -\omega_i\rho u_r/r, \quad (8)$$

$$S_i^{(2)} = \frac{\omega_i}{2r}[\partial_\beta(p\delta_{r\beta} + \rho u_\beta u_r)] + 3\omega_i\left[\frac{\rho\nu}{r}\left(\partial_r u_\beta - \frac{u_r}{r}\delta_{r\beta}\right)e_{i\beta} - \frac{\rho u_\beta u_r}{r}e_{i\beta}\right] - \omega_i(1-\tau)\partial_\beta(\rho u_r/r)e_{i\beta}. \quad (9)$$

They are basically identical as those in Refs. [9,10]; the minor difference is also illustrated in Appendix A.

For method B, the derivation begins from a fixed general format of the source term S_i [13] and the trapezium rule is used to integrate the Boltzmann equation. If the second-order integration is applied to the collision and source term [13], the LBE is

$$f_i(\mathbf{x}+\mathbf{e}_i\delta_t, t+\delta_t) - f_i(\mathbf{x},t) = \frac{1}{2}[\Omega_i|_{(\mathbf{x},t)} + \Omega_i|_{(\mathbf{x}+\mathbf{e}_i\delta_t, t+\delta_t)}] + \frac{1}{2}\delta_t[S_i|_{(\mathbf{x},t)} + S_i|_{(\mathbf{x}+\mathbf{e}_i\delta_t, t+\delta_t)}], \quad (10)$$

where $\Omega_i=-\frac{f_i-f_i^{eq}}{\tau'}$. To make the evolution (10) in an explicit form, a new density distribution function $\bar{f}_i$ is introduced as [13]

$$\bar{f}_i = f_i - \frac{1}{2}\Omega_i - \frac{1}{2}\delta_t S_i. \quad (11)$$

Hence, the evolution equation for $\bar{f}_i$ is [13]

$$\bar{f}_i(\mathbf{x}+\mathbf{e}_i\delta_t, t+\delta_t) - \bar{f}_i(\mathbf{x},t) = \bar{\Omega}_i|_{(\mathbf{x},t)} + \frac{\tau'}{\tau'+0.5}\delta_t S_i|_{(\mathbf{x},t)}, \quad (12)$$

where $\bar{\Omega}_i=-\frac{\bar{f}_i-\bar{f}_i^{eq}}{\tau'+0.5}$ and $\bar{f}_i^{eq}=f_i^{eq}$. In this LBE, the kinetic viscosity ν is defined as $\nu=c_s^2\tau'$ [13] and $\tau'=\tau-0.5$. Notice, there is a coefficient $\frac{\tau'}{\tau'+0.5}=(1-\frac{1}{2\tau})$ before the source term $\delta_t S_i$. Equation (12) is the *actual* LBE used in our numerical LBM code when we study the model B.

From Eqs. (5) and (11), the momentum of fluid ρu_α is defined as

$$\rho u_\alpha = \sum_i e_{i\alpha}\left(\bar{f}_i + \frac{1}{2}\Omega_i + \frac{1}{2}\delta_t S_i\right) = \sum_i e_{i\alpha}f_i^{eq}. \quad (13)$$

From the above equation and Eq. (7), we further obtained

$$\rho u_\alpha = \sum_i e_{i\alpha}\bar{f}_i + \frac{1}{2}\delta_t\sum_i e_{i\alpha}S_i = \rho u_\alpha^* + \frac{1}{2}\delta_t\sum_i e_{i\alpha}S_i. \quad (14)$$

Hence, in the method B, the common momentum of fluid ρu^*_α obtained from $\rho u^*_\alpha = \Sigma_i e_{i\alpha} \bar{f}_i$ should be altered as ρu_α in Eq. (14) and the EDF should be calculated with this altered velocity. At the same time, the density ρ is defined as

$$\rho = \sum_i \left(\bar{f}_i + \frac{1}{2}\Omega_i + \frac{1}{2}\delta_t S_i\right) = \sum_i \bar{f}_i^{eq} = \sum_i \bar{f}_i + \frac{1}{2}\delta_t \sum_i S_i, \tag{15}$$

which is different from the common formula $\rho = \Sigma_i \bar{f}_i$.

In the derivation of Premnath and Abraham [11], the forcing term S_i is written in a fixed form $S_i = \frac{F_\alpha(e_{i\alpha}-u_\alpha)}{\rho RT} f_i^{eq}$ [13], where F_α is the function of the body force in NS equations. Through the Chapman-Enskog expansion, to recover the NS equations, Premnath and Abraham [11] obtained the first and second source terms as

$$S_i^{(1)} = -\omega_i \rho u_r / r,$$

$$S_i^{(2)} = \frac{(e_{i\alpha}-u_\alpha)}{\rho c_s^2} f_i^{eq} \left[\frac{\nu}{r}\partial_r(\rho u_\alpha) - \frac{\rho \nu u_r}{r^2}\delta_{\alpha r} - \frac{\rho u_\alpha u_r}{r}\right]. \tag{16}$$

This model is referred as model B1.

On the other hand, deriving an axisymmetric model base on definitions of $\rho = \Sigma_i \bar{f}_i$ and $\rho u_\alpha = \Sigma_i e_{i\alpha} \bar{f}_i + \frac{1}{2}\delta_t \Sigma_i e_{i\alpha} S_i$ is also possible [4]. Here, we derived a model referred as model B2 using this strategy. In our derivation, the forcing term S_i is written in a power series in the particle velocity [14],

$$S_i = \omega_i \left\{A + \frac{e_{i\alpha} B_\alpha}{c_s^2} + \frac{C_{\alpha\beta}}{2c_s^2}\left(\frac{e_{i\alpha} e_{i\beta}}{c_s^2} - \delta_{\alpha\beta}\right)\right\}, \tag{17}$$

where A, B_α, and $C_{\alpha\beta}$ are functions of the body force in the NS equation. Through the Chapman-Enskog expansion, these functions can be obtained (refer to Appendix B).

For method C, the LBE is written as

$$f_i(\mathbf{x} + \mathbf{e}_i \delta_t, t + \delta_t) - f_i(\mathbf{x}, t) = -\frac{f_i - f_i^{eq}}{\tau} + \delta_t S_i|_{(\mathbf{x},t)}. \tag{18}$$

In the derivation, a centered scheme [15] is applied to the source terms $S_i|_{(\mathbf{x},t)}$ and it is written as $S_i|_{(\mathbf{x}+\mathbf{e}_i\delta_t/2, t+\delta_t/2)}$ [12].

Through the Taylor-series expansion, the source term can be written as $S_i|_{(\mathbf{x}+\mathbf{e}_i\delta_t/2, t+\delta_t/2)} = S_i|_{(\mathbf{x},t)} + \frac{1}{2}\delta_t(\partial_t + e_{i\beta}\partial_\beta)S_i$. It is noted that, the centered scheme [15] here does not necessarily mean that the derived model is implicit. Actually, the model is still an explicit one because the term $\frac{1}{2}\delta_t(\partial_t + e_{i\beta}\partial_\beta)S_i$ in the Taylor expansion would be eliminated in the derivation, while only the terms $S_i^{(1)}|_{(\mathbf{x},t)}$ and $S_i^{(2)}|_{(\mathbf{x},t)}$ appear finally.

Through the Chapman-Enskog expansion, to recover the NS equations, Zhou [12] obtained the constraints for first and second source terms as $\Sigma_i S_i^{(1)} = \frac{-\rho u_r}{r}$ and $\Sigma_i e_{i\alpha} S_i^{(2)} = \frac{-\rho u_\alpha u_r}{r} + \frac{\rho\nu}{r}(\partial_r u_\alpha - \frac{u_r}{r}\delta_{\alpha r})$. Zhou [12] choose source terms as $S_i^{(1)} = \frac{-\rho u_r}{9r}$ and $S_i^{(2)} = \frac{e_{i\beta}}{6}[\frac{-\rho u_\beta u_r}{r} + \frac{\rho\nu}{r}(\partial_r u_\beta - \frac{u_r}{r}\delta_{\beta r})]$. Actually, more naturally, $S_i^{(1)}, S_i^{(2)}$ can be written as $S_i^{(1)} = \frac{-\omega_i \rho u_r}{r}$ and $S_i^{(2)} = \frac{\omega_i}{c_s^2} e_{i\beta}[\frac{-\rho u_\beta u_r}{r} + \frac{\rho\nu}{r}(\partial_r u_\beta - \frac{u_r}{r}\delta_{\beta r})]$ since they all satisfy the constraints.

B. Minor-type errors in existed models

As discussed in above section, the existed axisymmetric models can be classified as three groups. Here, we would discuss the minor errors in existed models which derived using methods A and B.

In the derivation of Reis and Phillips [9,10], there are some type errors. The first one is their Eq. (36) should be $P_{\alpha\beta\gamma} = \rho c_s^2(u_\gamma \delta_{\alpha\beta} + u_\alpha \delta_{\beta\gamma} + u_\beta \delta_{\alpha\gamma})$. In the following part, to compare directly with relevant equations in Refs. [9,10], subscript "y" while not "r" is used although they all stand for the axial coordinate. Another type error is their Eq. (46) that should be

$$\begin{aligned}\left(2\nu - \frac{1}{6}\right)\frac{\rho\nu}{y}\left(\partial_y u_y - \frac{u_y}{y}\right) &= -\frac{1-12\nu}{6y}\left(-\frac{3Q_{yy}}{2\tau} - \frac{\rho u_y}{y}\right)\\ &= \frac{1-12\nu}{y}\left(\frac{Q_{yy}}{2(1+6\nu)} + \frac{\rho u_y}{6y}\right).\end{aligned} \tag{19}$$

where $Q_{\alpha\beta}$ is defined in Ref. [10] as $Q_{\alpha\beta} = \Sigma_i e_{i\alpha} e_{i\beta} f_i^{(neq)} = -\frac{\rho\tau}{3}(\partial_\alpha u_\beta + \partial_\beta u_\alpha)$ and $\rho \partial_y u_y = -\frac{3Q_{yy}}{2\tau}$. It is also noted that in the above derivation, equations $2\nu - \frac{1}{6} = -\frac{1-12\nu}{6}$ and $4\tau = 2(1+6\nu)$ are used. A detailed analysis in Appendix A and in Eq. (19) illustrate that there are some type errors in the very last equations in Refs. [9,10]. They should be

$$\begin{aligned}S_i^{(2)} = {}& \frac{3\omega_i}{y}\frac{e_{iy}^2}{2}\left(\rho u_x \partial_x u_y - \frac{3u_y\omega}{2}Q_{xx} - 3u_y\omega Q_{yy} + \frac{\partial_y \rho}{3}\right)\\ &- \frac{3\omega_i}{y}e_{ix}\left(\frac{6\nu}{6\nu+1}Q_{xy} + \frac{\rho}{6}\partial_x u_y - \rho u_x u_y\right)\\ &+ \frac{3\omega_i}{y}e_{iy}\left[(1-12\nu)\left(\frac{1}{2(1+6\nu)}Q_{yy} + \frac{\rho u_y}{6y}\right) - \rho u_y^2\right].\end{aligned} \tag{20}$$

It is noted that here $\omega = \frac{1}{\tau}$, which is different from the weighting factor ω_i.

For the model of Premnath and Abraham [11], the trapezium rule is used to integrate the Boltzmann equation, but the forcing-term formula [11,13] is inconsistent with the second-order truncation error in LBM [12]. In Ref. [11], there is a type error in the axisymmetric NS equation [i.e., Eq. (2) in Ref. [11]], where the term $-2\mu\frac{u_r}{r^2}$ is missing and so as the second source term.

III. NUMERICAL STUDY

In this section, we would like to make a comparison of accuracy and τ sensitivity of the three-type models. In this numerical study, two flows would be simulated. One is the flow through a constricted tube (Fig. 1); the other is the flow over an axisymmetrical sphere placed in a 3D circular tube

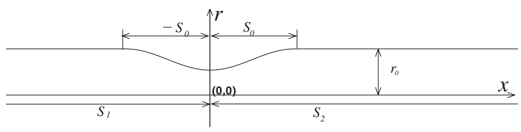

FIG. 1. Geometry of constricted tubes.

(Fig. 5). These flows are applicable to test the accuracy of the models because not only u_x but also u_r is important in the vicinity of the constrictions.

For the first flow, the geometry of the constrictions is described by the cosine curve, which is shown in Fig. 1. If r_0 is the radius of the nonstenotic part of the pipe, the radius of the stenose $r(x)$ is described as

$$r(x) = r_0 - \beta r_0\{1 + \cos[\pi x/S_0]\}/2 \quad (-S_0 < x < S_0),$$

where $r_0=D/2$, $\beta=50\%$ is the severity of stenose, and the axial length of the stenose is $2S_0$. To make the flow fully developed and save grid nodes, the upstream (inlet) and downstream (outlet) boundaries are at $S_1=-3D$ and $S_2=8D$ as illustrated in Fig. 1.

As we know, there are three popular curved-wall boundary treatments: the nonequilibrium-extrapolation (Guo's method) [16], the momentum transfer (Bouzidi's method) [18], and the bounce-back-extrapolation method (Yu's method) [17]. In our simulations, all these boundary methods were applied to see the effect of different boundary conditions.

For the inlet/outlet boundary conditions, the pressure or velocity boundary-condition treatment [20] was adopted for its simplicity. At the inlet boundary, a fully developed parabolic velocity profile is specified. In the outlet boundary, the outlet pressure was specified and $\partial \mathbf{u}/\partial x=0$ was also imposed [21]. The gradient terms contained in the source terms are evaluated by the second-order central difference method.

For the axisymmetric boundary conditions, the slip wall boundary condition was used [8]. The source terms on these lattice nodes are not necessary to be known. Hence, the singularity problem is avoided.

In all of our simulations, Reynolds number defined as $\mathrm{Re}=U_0D/\upsilon$, where U_0 is the central value of the inlet parabolic velocity. The zero velocities are initialized everywhere. In defining the steady state, our criterion is

$$\eta = \sum_{i,j} \frac{\|\mathbf{u}(x_i,r_j,t+\delta_t) - \mathbf{u}(x_i,r_j,t)\|}{\|\mathbf{u}(x_i,r_j,t+\delta_t)\|} < 10^{-6},$$

where the summation is over the entire system.

For the first flow, all models (models A, B1, B2, and C) with different boundary-condition treatments [16–18] are used to simulate the same case with $S_0=D$, $\mathrm{Re}=10$. In the simulation, first a uniform grid with $N_x \times N_r = 441 \times 22$ (N_r is the lattice nodes in radial direction) was used. The nonstenotic radius is represented by 21 lattice nodes and N_r includes one extra layer beyond the wall boundary. One of the results obtained by model C with $\tau=0.8$ and Yu's wall boundary condition [17] was illustrated in Fig. 2. In the figure, the velocity profiles in positions $x=0$, $0.5D$, D, and $2D$ are compared with those of the finite-volume method (FVM). Both the axial and radial velocity components obtained from the LBM agree well with those of the FVM. Notice, here the results obtained by the FVM are regarded as accurate results because a very fine grid (i.e., 1321×61) is used in FVM simulations. It is found that all models are able to give accurate results which looks like Fig. 2.

In the following section, we would discuss the accuracy issue of these models. Here, a variable E is defined to measure the discrepancies between the velocities obtained from LBM and FVM,

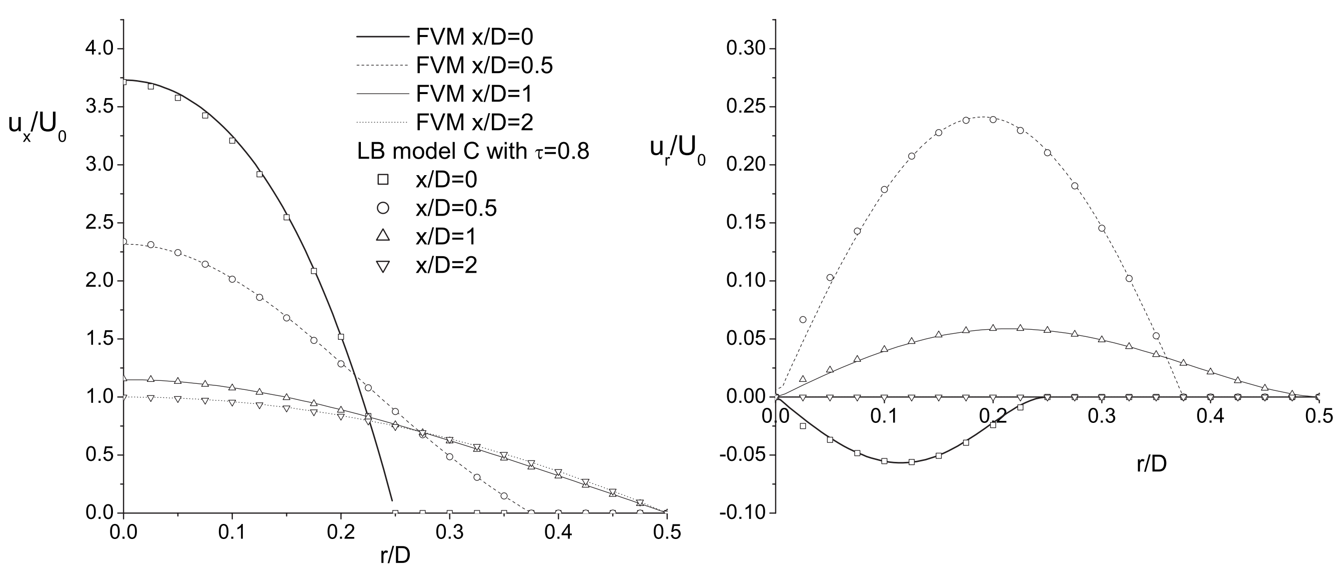

FIG. 2. Velocity profiles in different position in case of $\mathrm{Re}=10$. In the LB simulation, model C is applied with the Yu's boundary-condition treatment [17] and $\tau=0.8$.

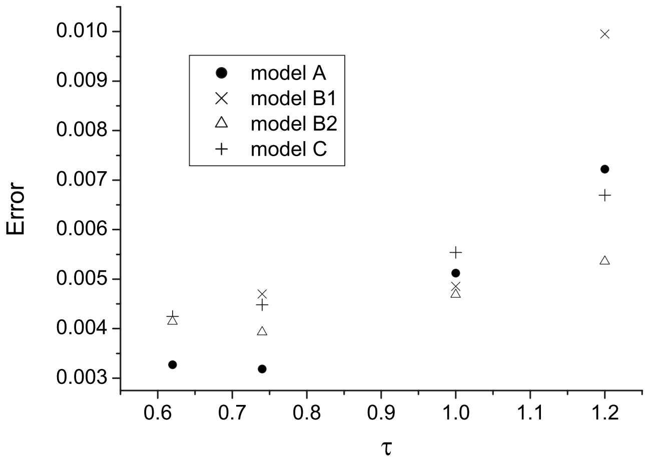

FIG. 3. The error as a function of the relaxation time τ; the case of Re=10 was simulated using models A, B1, B2, and C with mesh 441×22. Guo's method was applied for the wall boundary treatment.

$$E=\frac{\sum_{i,j}|u_x(x_i,r_j)-u_{ax}(x_i,r_j)|}{\sum_{i,j}|u_{ax}(x_i,r_j)|}, \tag{21}$$

where $u_x(x_i,r_j)$ is the axial velocity on the discrete lattice point (x_i,r_j) and $u_{ax}(x_i,r_j)$ is the accurate axial velocity obtained through the FVM. The summation in Eq. (21) is only over the total 46 lattice nodes in positions $x=0$, $0.5D$, D, and $2D$ (refer to the left graph of Fig. 2). Here, the case was simulated using the four models with different relaxation time. The error [i.e., Eq. (21)] as a function of the relaxation time is illustrated in Fig. 3. It is found that the errors are all very small and the error trends of all models are similar.

Guo's, Yu's, and Bouzidi's curved-wall boundary treatments are all found on the second-order accuracy in space [16–18]. Here, the spatial accuracy for the axisymmetric-flow simulations was studied. Figure 4 illustrates the numerical error [Eq. (21)] as a function of lattice nodes in tube's radius N_r when model A is used to simulate the case. We can see that all the spatial accuracy is around the second order. In our simulations when finer meshes or the τ changes, the U_0 can be changed so as to make simulated Reynolds number fixed because $\mathrm{Re}=2U_0N_r\delta_x/[c_s^2\delta_t(\tau-0.5)]$. It is also found when applying models B1, B2, and C, the spatial accuracies of these boundary treatments are all consistent with the LBM (second-order accuracy).

Then, we would like to compare which model is more stable. The "stable" in the paper means that the model's computational stability is not sensitive to τ. As we know, when τ is close to 0.5, the numerical instability may appear. In our study, how stable a LB model is demonstrated by the minimum τ value at which the numerical instability does not appear. The τ sensitivity may be dependent on the model as well as the boundary conditions and flow. To evaluate the effect of the boundary conditions and flow, in the following studies, all boundary conditions and the two different flows were used.

Although it is hard to find out the exact $\tau_{\min}$ numerically, here we obtained $\tau_{\min}$ with an accuracy of ± 0.005 since we tried to find the $\tau_{\min}$ from $\tau=1.0$ with a decreasing step size of 0.005. The $\tau_{\min}$ values of these models are listed in Table I. From Table I, we can see that even $\tau_{\min}=0.52$, the computation of model C is still stable when Yu's [17] or Guo's [16] boundary condition is applied. Compared with Yu's and Guo's method, Bouzidi's method slightly makes the computations of models B1, B2, and C less stable. It is found that for any boundary treatment, $\tau_{\min}$ of model C [12] is the smallest one. It seems that Zhou's model [12] is the most stable one among these four models.

Form Table I, it is also found that model B2 is more stable than model B1. As the main difference between these two models is the density definition, for model B1, $\rho=\Sigma_i\bar{f}_i+\frac{1}{2}\delta_t\Sigma_i S_i$ while in model B2, $\rho=\Sigma_i\bar{f}_i$; it seems a usual defi-

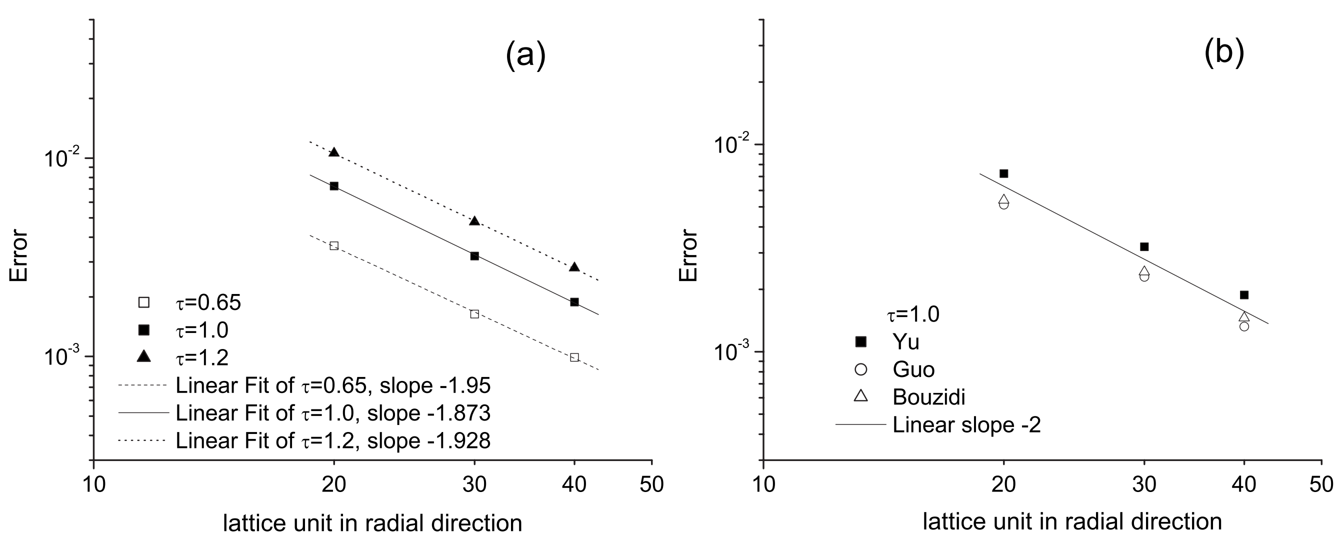

FIG. 4. The error as a function of the tube's radius N_r when model A is used to simulate the case of Re=10. (a) Yu's [17] curved-wall boundary treatment was applied but $\tau=0.65$, 1.0, and 1.2, respectively. (b) Yu's [17], Guo's [16], and Bouzidi's [18] curved-wall boundary treatments were applied, respectively, with $\tau=1$.

TABLE I. $\tau_{\min}$'s for the four models when the flow through a constricted tube was simulated with mesh 441×22.

	Model A[a]	Model B1[b]	Model B2	Model C[c]
Yu[d]	0.615	0.625	0.535	0.515
Guo[e]	0.615	0.625	0.535	0.515
Bouzidi[f]	0.615	0.645	0.555	0.555

[a]Reference [7].
[b]Reference [11].
[c]Reference [12].
[d]Reference [17].
[e]Reference [16].
[f]Reference [18].

nition on the density of fluid without being directly relevant to source terms may make a LB model more stable.

It is also found that when 881×42 mesh is used for the same flow, the measured $\tau_{\min}$'s are almost identical to those in Table I which are obtained by using mesh 441×22. The mesh size seems not to affect the τ sensitivity.

To further compare which model is more stable in terms of τ sensitivity, here another flow over an axisymmetrical sphere placed in a 3D circular tube is also studied. In our numerical study, the flow field is assumed axisymmetric. The geometry of the ball and circular tube is illustrated in Fig. 5. The diameter and length of the tube are D and $L=10D$, respectively, while the diameter of the ball is $D/2$. In all our LBM simulations, a uniform grid with $N_x\times N_r=601\times32$ was used. In the following studies, only the case of Re $=100$ is simulated.

In Fig. 6, it is found that the axial velocity profiles obtained from the LBM agree well with those obtained by the FVM. The LBM result is obtained from model A with the Yu's boundary condition and $\tau=0.61$. All the models with the three boundary conditions are able to give accurate results as Fig. 6.

The measured $\tau_{\min}$ values which have an accuracy of ±0.005 are listed in Table II. From Table II, we can see that this time the $\tau_{\min}$'s of each model are almost independent on the boundary conditions. Again, it is found that no matter what the three boundary conditions was applied, $\tau_{\min}$ of model C [12] is the smallest one.

It is noted that most partial derivatives in the source term are also able to be evaluated by the second moments of the nonequilibrium distribution functions [7,9,10,21]. If this evaluation method is applied, $\partial_x u_r$ still has to be evaluated by the finite difference [7,9,10,21]. Our numerical tests show that $\tau_{\min}$'s obtained through this evaluation method are identical as those obtained through the second-order central finite

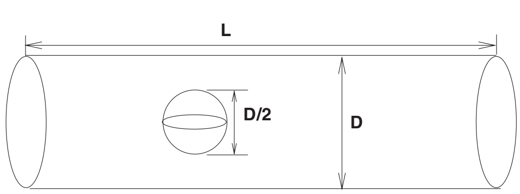

FIG. 5. Geometry of the flow over an axisymmetrical sphere placed in a 3D circular tube.

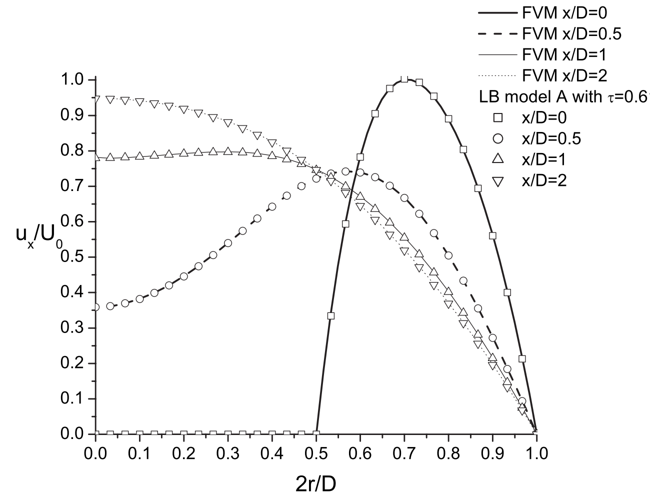

FIG. 6. Velocity profiles in different position for flows over an axisymmetrical sphere placed in a 3D circular tube with Re=100, mesh 601×32, and $\tau=0.61$. Yu's curved-wall boundary treatment was applied.

difference. These two evaluation methods have no significant influences on the numerical stability in terms of τ sensitivity.

Furthermore, our numerical tests show that the source term chosen as that in Refs. [9,10] or in Ref. [7], which is illustrated in Appendix A, makes no difference in terms of τ sensitivity.

IV. CONCLUSION

Through theoretical and numerical analyses of three-type axisymmetric lattice Boltzmann D2Q9 models, it is found that all these models are able to mimic the 2D Navier-Stokes equation in the cylindrical coordinates accurately. However, as a centered scheme is applied to the source terms, the derivation procedure of method C [12] seems the simplest one. Applying a centered scheme to the source terms may make the derivation of the forcing term in the LBM simple. At the same time, in terms of sensitivity to τ, the model of Zhou [12] is the most stable model. It is also found that if the density of fluid is defined in its usual way and not directly relevant to source terms, the lattice Boltzmann model seems more stable.

TABLE II. $\tau_{\min}$'s of the four models when the flow over an axisymmetrical sphere placed in a 3D circular tube was simulated with mesh 661×32.

	Model A[a]	Model B1[b]	Model B2	Model C[c]
Yu[d]	0.605	0.615	0.535	0.515
Guo[e]	0.605	0.625	0.535	0.515
Bouzidi[f]	0.605	0.625	0.535	0.515

[a]Reference [7].
[b]Reference [11].
[c]Reference [12].
[d]Reference [17].
[e]Reference [16].
[f]Reference [18].

APPENDIX A

The constraints for the first and second source terms, which are obtained through method A are [7]

$$\sum_i S_i^{(1)} = -\frac{\rho u_r}{r}, \quad \sum_i e_{i\alpha} S_i^{(1)} = 0, \tag{A1}$$

$$\sum S_i^{(2)} = \frac{1}{2r}\partial_\beta(p\delta_{r\beta}+\rho u_\beta u_r), \tag{A2}$$

and

$$\sum_i S_i^{(2)} e_{i\alpha} = -c_s^2(1-\tau)\partial_\alpha(\rho u_r/r) + \frac{\nu}{r}\left(\partial_r \rho u_\alpha - \frac{1}{r}\rho u_r \delta_{r\alpha}\right) - \frac{\rho u_\alpha u_r}{r}. \tag{A3}$$

Notice, in the derivation of Reis and Phillips [9,10], $-c_s^2(1-\tau)=\nu-\frac{1}{6}$. Hence, from Eq. (A3), we have

$$\sum_i S_i^{(2)} e_{i\alpha} = \left(\nu - \frac{1}{6}\right)\partial_\alpha\left(\frac{\rho u_r}{r}\right) + \frac{\nu}{r}\left(\partial_r \rho u_\alpha - \frac{1}{r}\rho u_r \delta_{r\alpha}\right) - \frac{\rho u_\alpha u_r}{r}. \tag{A4}$$

In Eq. (A4), suppose $\alpha=x$ and $\alpha=r$, it is straightforward to get Eqs. (43) and (44) in Ref. [10], respectively. Hence, the constraints for source terms in Refs. [7,9,10] are identical. As we know, there are two constraints and nine $S_i^{(2)}$ unknowns. There are many possible solutions. Typically, the unknown $S_i^{(2)}$'s are chosen as

$$S_i^{(2)} = 3\omega_i\left[e_{ir}^2\left(\sum_i S_i^{(2)}\right) + e_{ix}\left(\sum_i S_i^{(2)} e_{ix}\right) + e_{ir}\left(\sum_i S_i^{(2)} e_{ir}\right)\right]$$

in Refs. [9,10] and

$$S_i^{(2)} = \omega_i\left(\sum_i S_i^{(2)}\right) + 3\omega_i\left[e_{ix}\left(\sum_i S_i^{(2)} e_{ix}\right) + e_{ir}\left(\sum_i S_i^{(2)} e_{ir}\right)\right]$$

in Ref. [7]. It is easy to understand that these choices all satisfy the constraints on $S_i^{(2)}$. Another slight difference between the models of Reis and Phillips [9,10] and Lee *et al.* [7] is that most derivatives in $S_i^{(2)}$ are described as a function of $Q_{\alpha\beta}$ (refer to Sec. II B), except as a partial derivative $\partial_x u_r$, which has to be evaluated by the finite difference [6,9].

APPENDIX B

When the trapezium rule is used to integrate the Boltzmann equation [i.e., Eq. (12)] and the forcing term S_i is written in a power series in the particle velocity [i.e., Eq. (17)], to recover the NS equations correctly, $A^{(1)}$, $B_\alpha^{(1)}$, $A^{(2)}$, $B_\alpha^{(2)}$, and $C_{\alpha\beta}^{(1)}$ should be chosen as follows:

$$A^{(1)} = -\rho u_r/r, \quad B_\alpha^{(1)} = -\rho u_\alpha u_r/r, \tag{B1}$$

$$A^{(2)} = \partial_\beta(p\delta_{r\beta}+\rho u_\beta u_r)/2r,$$
$$B_\alpha^{(2)} = -(\tau-1)c_s^2\partial_\alpha A^{(1)} + \frac{\rho\nu}{r}\left(\partial_r u_\alpha - \frac{u_r}{r}\delta_{\alpha r}\right), \tag{B2}$$

$$C_{\alpha\beta}^{(1)} = 2u_\alpha B_\beta^{(1)} \quad \text{or} \quad C_{\alpha\beta}^{(1)} = u_\alpha B_\beta^{(1)} + u_\beta B_\alpha^{(1)}, \tag{B3}$$

and the final formula of S_i can be written as

$$S_i = \omega_i\left\{\frac{A^{(1)}}{n} + \frac{e_{i\alpha}B_\alpha^{(1)}}{c_s^2} + \frac{C_{\alpha\beta}^{(1)}}{2c_s^2}\left(\frac{e_{i\alpha}e_{i\beta}}{c_s^2} - \delta_{\alpha\beta}\right)\right\} + \omega_i\delta_t\left\{\frac{A^{(2)}}{n} + \frac{e_{i\alpha}B_\alpha^{(2)}}{c_s^2}\right\}, \tag{B4}$$

where $n=(1-\frac{1}{2\tau})$.

[1] G. McNamara and G. Zanetti, Phys. Rev. Lett. **61**, 2332 (1988).
[2] F. Higuera and J. Jimenez, Europhys. Lett. **9**, 663 (1989).
[3] J. M. Buick and C. A. Greated, Phys. Rev. E **61**, 5307 (2000).
[4] Z. Guo, C. Zheng, and B. Shi, Phys. Rev. E **65**, 046308 (2002).
[5] L.-S. Luo, Phys. Rev. Lett. **81**, 1618 (1998).
[6] I. Halliday, L. A. Hammond, C. M. Care, K. Good, and A. Stevens, Phys. Rev. E **64**, 011208 (2001).
[7] T. S. Lee, H. Huang, and C. Shu, Int. J. Mod. Phys. C **17**, 645 (2006).
[8] Y. Peng, C. Shu, Y. T. Chew, and J. Qiu, J. Comput. Phys. **186**, 295 (2003).
[9] T. Reis and T. N. Phillips, Phys. Rev. E **75**, 056703 (2007).
[10] T. Reis and T. N. Phillips, Phys. Rev. E **76**, 059902 (2007).
[11] K. N. Premnath and J. Abraham, Phys. Rev. E **71**, 056706 (2005).
[12] J. G. Zhou, Phys. Rev. E **78**, 036701 (2008).
[13] X. He, S. Chen, and G. D. Doolen, J. Comput. Phys. **146**, 282 (1998).
[14] A. J. C. Ladd and R. Verberg, J. Stat. Phys. **104**, 1191 (2001).
[15] J. G. Zhou, *Lattice Boltzmann Methods for Shallow Water Flows* (Springer-Verlag, Berlin, 2004).
[16] Z. Guo, C. Zheng, and B. Shi, Phys. Fluids **14**, 2007 (2002).
[17] D. Yu, R. Mei, and W. Shyy, AIAA J. **2003**, 953 (2003).
[18] M. Bouzidi, M. Firdaouss, and P. Lallemand, Phys. Fluids **13**, 3452 (2001).
[19] L. D. Landau and E. M. Lifschitz, *Fluid Mechanics*, 2nd ed. (Pergamon, Oxford, 1987).
[20] Z. Guo, C. Zheng, and B. Shi, Chin. Phys. **11**, 366 (2002).
[21] T. S. Lee, H. Huang, and C. Shu, Int. J. Numer. Methods Fluids **49**, 99 (2005).